Arabian Journal of Chemistry (2019) 12, 881–896

King Saud University

Arabian Journal of Chemistry

www.ksu.edu.sa
www.sciencedirect.com

ORIGINAL ARTICLE

Crystal structure, conformation and vibrational characteristics of diethyl 4,4′-disulfanediylbis (6-methyl-2-phenylpyrimidine-5-carboxylate) – A new pharmaceutical cure

Wojciech Sąsiadek [a,*], Iwona Bryndal [a,c], Jadwiga Lorenc [a], Maciej Ptak [b], Jerzy Cieplik [c], Marcin Stolarczyk [c], Tadeusz Lis [d], Jerzy Hanuza [b]

[a] *Department of Bioorganic Chemistry, Institute of Chemistry and Food Technology, Faculty of Engineering and Economics, Wrocław University of Economics, 118/120 Komandorska, 53-345 Wrocław, Poland*
[b] *Institute of Low Temperature and Structure Research, Polish Academy of Sciences, 2 Okólna, 50-422 Wrocław, Poland*
[c] *Faculty of Pharmacy with Division of Laboratory Diagnostics, Wrocław Medical University, 211 Borowska, 50-556 Wrocław, Poland*
[d] *Faculty of Chemistry, University of Wrocław, 14 Joliot-Curie, 50-383 Wrocław, Poland*

Received 30 September 2015; accepted 15 March 2016
Available online 22 March 2016

KEYWORDS

Disulfide bond;
6-Methyl-2-phenylpyrimidine derivatives;
IR and Raman spectroscopy;
X-ray diffraction;
Synthesis;
Quantum chemical calculation

Abstract The crystal and molecular structures of diethyl 4,4′-disulfanediylbis(6-methyl-2-phenyl pyrimidine-5-carboxylate) have been determined by X-ray diffraction and quantum chemical DFT analysis. The title compound crystallizes in orthorhombic Pbca (D_{2h}^{15}) space group, with one molecule in the asymmetric unit. The molecular structure of the studied compound has been determined using the DFT B3LYP/6-311G(2d,2p) approach and compared to that derived from X-ray studies. The IR and Raman spectra have been measured and their wavenumbers have been compared to those calculated for the optimized geometry of the studied compound. The characteristic vibrations of the 4,4′-dithiobispyrimidine N_2C_4—S—S—C_4N_2 skeleton have been identified and on this basis the correlation between the disulfide bridge conformation and vibrational data have been discussed.

* Corresponding author. Tel.: +48 71 3680299; fax: +48 71 3680292.
E-mail address: wojciech.sasiadek@ue.wroc.pl (W. Sąsiadek).
Peer review under responsibility of King Saud University.

ELSEVIER Production and hosting by Elsevier

http://dx.doi.org/10.1016/j.arabjc.2016.03.004
1878-5352

1. Introduction

The heterocyclic pyrimidine ring is the basis of a wide class of natural compounds. It appears as a substituted or fused compound forming a great number of pyrimidine derivatives. It is found in nucleotides, thiamine, uric acid, alloxan, barbiturates and HIV drugs. Since its discovery and laboratory synthesis, the pyrimidine derivatives have become the essential structural unit of wide range pharmaceuticals having important biological, antimicrobial and anticancer activities (Cieplik et al., 2015; Cocco et al., 1995, 2001; Cunha et al., 2007). Thioxopyrimidine has become lately a very important unit occurring in a new class of pharmaceuticals (Cieplik et al., 2015; Cocco et al., 2001; Cunha et al., 2007). New ways of the syntheses were proposed for 4-thiopyrimidines (Cunha et al., 2007), diethyl 4,4′-disulfanediyl bis(6-methyl-2-phenylpyrimidine-5-carboxylate), tetrasulfane-1,4-diylbis-(6-methyl-2-phenlpyrimidine-4,5-diyl)dimethanol as well as diethyl 4,4′-disulfanediylbis[6-(methoxycarbotionyl)-2-phenylpyrimidine-5-carboxylate] (Cieplik et al., 2015). All these compounds contain the skeleton in which the central pyrimidine ring is substituted in the C2 position by phenyl unit, in the C4 position by disulfide or tetrasulfane fragment, in the C5 position by carboxyl unit and in the C6 position by methyl group. It means, that the essential fragment of these compounds is the N_2C_4—S—S—C_4N_2 skeleton that determines all properties of this class of pharmaceuticals. A similar skeleton was found in 5-phenyl-3-(4-cyano-5-phenylisothiazol-3-yl) disulphanyl-4-isothiaolecarbonitrile (Romani et al., 2015) but the disulfide skeleton connects different rings in it. The reported vibrational data in this paper were related to those obtained here, but it was not possible to compare the structures of both compounds due to lack of full structural parameters in the paper by Romani et al. (2015).

The aim of the present work was to characterize crystal and molecular structures of diethyl 4,4′-disulfanediylbis(6-methyl-2-phenylpyrimi dine-5-carboxylate), abbreviated as **DSMP**, as well as its vibrational characteristics determined from IR and Raman spectra measurements and quantum chemical DFT calculations. We used a different procedure for the synthesis and solvent crystallization of **DSMP** than described by Cunha et al. (2007), which could be the cause of obtaining a second polymorph of **DSMP**. The synthesized compound in the present work is new and representative for a wide class of lately studied thioxopyrimidine pharmaceuticals (Cieplik et al., 2015; Cunha et al., 2007). They have a specific chemical composition and structure and the recognition of their vibrational properties is important for analytical purposes.

Vibrational spectroscopy is an excellent tool for studying the content of active substances in plants and pharmaceuticals. The crucial problem in the discussion of recorded IR and Raman spectra is discrimination of characteristic for these compounds bands from other lines appearing in the spectra. This is often difficult and speculative if we do not have the proper data on their vibrational characteristics.

2. Experimental

2.1. Synthesis

The general method for the synthesis of **DSMP** using ethyl 4-methyl-2-phenyl-6-sulfanylpyrimidine-5-carboxylate as a substrate was mentioned in our previous work (Cieplik et al., 2015). 4 g (0.010 mmol) of this substrate was dissolved in 50 cm^3 of tetrahydrofuran. The mixture was refluxed for 8 h with the presence of phenylhydrazine, and then it was cooled and poured into 100 cm^3 cold water. The obtained compound was purified by crystallization from methanol to give yellow crystals yielding 4.2 g (25%). In this procedure, only one polymorph of **DSMP** is formed – the orthorhombic form. The results of chemical analysis of **DSMP** ($C_{28}H_{26}N_4O_4S_2$) are : C 61.53% (theor. 61.51%), H 4.75% (4.79%), N 10.18% (10.24%). Its melting point: 129–130 °C and molecular weight: 546.65.

2.2. IR and Raman measurements

IR spectra in the 4000–40 cm^{-1} range were recorded at room temperature in Nujol and Fluorolube suspensions and KBr pellet with a FTIR Biorad 575C spectrometer. They were identical in the ranges where the bands of Nujol or Fluorolube are absent, so the IR spectra measured in KBr are shown in this paper. The resolution was 2.0 cm^{-1}.

Raman spectra in the 4000–80 cm^{-1} range were measured in back scattering geometry with a FT Bruker 110/S spectrometer. The resolution was 2.0 cm^{-1}. The YAG:Nd^{3+} (excitation wavelength 1064 nm) laser was used as an excitation source.

2.3. X-ray data collection

Crystallographic measurements for the **DSMP** were performed on a κ-geometry Oxford Diffraction Xcalibur PX KM-4-CCD diffractometer with graphite-monochromatized Mo Kα radiation (λ = 0.71073 Å) at 90(2) K, using an Oxford-Cryosystems cooler. Data collection, cell refinement, and data reduction and analysis were carried out with the Xcalibur PX software (Oxford Diffraction, Poland): CRYSALISCCD and CRYSALISRED, respectively (Oxford Diffraction Ltd., 2009).

The structure was solved by direct methods using the SHELXS-97 program (Sheldrick, 2008) and refined on F^2 by full-matrix least squares with anisotropic thermal parameters for all non-H atoms using SHELXL-97 (Sheldrick, 2008). All H atoms were found in difference Fourier maps and were refined isotropically. In the final refinement cycles, the C-bonded H atoms were positioned geometrically and treated as riding atoms, with C—H = 0.95–0.99 Å, and with U_{iso}(H) = 1.2U_{eq}(C) for CH and CH_2 or 1.5U_{eq}(C) for CH_3. The N-bonded H atom was refined with U_{iso}(H) = 1.2U_{eq}(N). The figures were made using the DIAMOND program (Brandenburg, 2005).

Crystal data for **DSMP**: $C_{28}H_{26}N_4O_4S_2$, M = 546.65, orthorhombic (No. 61), space group Pbca (D_{2h}^{15}), a = 16.829 (5), b = 15.125 (4), c = 20.728 (6) Å, V = 5276 (3) $Å^3$, Z = 8, T = 90(2) K, 57595 measured reflections, 7652 independent reflections (R_{int} = 0.029), 6537 reflections with $I > 2\sigma(I)$, S = 1.05, θ_{max} = 30°, $R[F^2 > 2\sigma(F^2)]$ = 0.033, $wR(F^2)$ = 0.086, $\Delta\rho_{max}$ = 0.40 e $Å^{-3}$, $\Delta\rho_{min}$ = −0.25 e $Å^{-3}$.

The powdered crystal of **DSMP** diffraction data were recorded at room temperature on a D8 ADVANCE powder diffractometer with nickel-filtered Cu Kα radiation (λ = 1.5418 Å) and a Vantec detector. The measurements were performed within 2θ range of 10–115° with a scan rate 0.008° per step and counting time of 4 s per step. X-ray powder diffraction pattern of **DSMP** was compared with the simulated XRD pattern of single crystal of the polymorph obtained byCunha et al. (2007). The simulated XRD pattern was obtained with a use of the CCDC's *Mercury program* (Macrae et al., 2006) and compared to that of new polymorph obtained by us.

2.4. Quantum chemical calculations

The geometry optimization of the molecular structure of the studied compound was performed for the monomeric unit using Gaussian 03 program package (Frisch et al., 2003). In the calculations the atomic positions from X-ray studies were taken as input data. Only one stable conformer with zero vibrational potential energy was found in such an approach. All calculations were performed applying density functional three-parameter hybrid (B3LYP) methods (Becke, 1996; Lee et al., 1988; Parr and Yang, 1989) with the 6-311G(2d,2p) (McLean and Chendler, 1980; Krishnan et al., 1980) basis set, starting from the X-ray geometry. The calculated and experimental values were compared using two scaling factors (see Table 3) to correct the evaluated wavenumbers for vibrational anharmonicity and deficiencies inherent to the used computational level. The IR and Raman wavenumbers were calculated for a single molecule.

The Potential Energy Distribution (PED) of the normal modes among the respective internal coordinates was calculated using the BALGA program (M.J. Nowak, L. Lapinski), BALGA computer program for PED calculations (Rostkowska et al., 2009).

Vector displacements of the atoms from their equilibrium positions during vibration and the pictures of these displacements were prepared using the ChemCraft program that also visualizes particular modes in an animated way (Zhurko and Zhurko, ChemCraft 1.7).

A linear correlation was used for scaling the theoretical wavenumbers to compare them with the experimental values (Palafox and Rastogi, 2002). The scaling of the calculated wavenumbers improves this result to 2.4 cm^{-1} for the IR and the Raman spectra. 0.93 scaling factor was used for the range 3500–2500 cm^{-1} and 0.98 for the range 2499–0 cm^{-1} of the spectra. The root mean square deviation (RMSD) between the experimental and calculated unscaled wavenumbers for **DSMP** was 48.4 for the IR and 48.3 for the Raman spectra. The scaling of the calculated wavenumbers improves this result to 6.5 cm^{-1} for the IR and 5.6 for the Raman spectra.

The theoretical Raman intensities were calculated using the RAINT computer program (Michalska, 2002) reported in Michalska and Wysokiński (2005).

3. Results and discussion

3.1. Crystal structure

The formation of the crystalline **DSMP** in the new polymorph (orthorhombic form) of single crystals was confirmed by XRD measurements. The simulated XRD pattern of **DSMP** from the single crystal data of the triclinic form obtained by Cunha et al. (2007) (red), and of the orthorhombic form obtained by us (black), and the experimental XRD patterns of the powder orthorhombic form (blue) are presented in Fig. 1. We can see clear differences between simulated XRD patterns obtained for the single crystal data of the triclinic and orthorhombic forms. On the other hand, a good agreement appears between the simulated XRD patterns obtained for the orthorhombic single crystal and the experimental pattern of the powdered sample. The small difference between both patterns, particularly at high angles, can be explained as the results of the measurements at different temperatures (90 K and RT), but it is not caused by the phase transition. Such differences, a result of changes in unit cell parameters due to the lowering of temperature, are well known (Li et al., 2014; Wang et al., 2014; Yoshii et al., 2015).

DSMP crystallizes in Pbca space group, with one molecule in the asymmetric unit (Fig. 2). The primitive unit cell is built of eight molecules. Selected bond distances, bond angles and principal torsion angles are presented in Table 1. Geometrical parameters were compared with those derived from the DFT calculations and also with the data on the other polymorph – the triclinic form reported by Cunha et al. (2007). The former data are presented for verification of the theoretical model used in the calculations (three-parameter hybrid B3LYP methods with the 6-311G(2d,2p) basis set).

DSMP contains the S—S bond linking two identical fragments which are built of the phenyl ring, the methyl and the ethyl ester groups attached to the pyrimidine ring. The bond lengths S1—S1′ [2.0473(5) Å], S1—C4 [1.7952(11) Å] and S1′—C4′ [1.7927(12) Å] are compared with corresponding values observed in the previously described triclinic form of **DSMP** (Table 1) (Cunha et al., 2007). On the whole, bond distances and bond angles in the orthorhombic form are in accordance with the corresponding values of the triclinic form (Cunha et al., 2007). However, pronounced differences between both polymorphs are apparent in the conformation of the pyrimidine rings in relation to each other and also in the conformation of ethyl ester groups and phenyl rings in relation to pyrimidine rings. A comparison of the molecular structures of both polymorphs of **DSMP** is shown in Fig. 3.

The conformation of **DSMP** is best defined by the torsion angles C4—S1—S1′—C4′, S1′—S1—C4—N3 and S1′—S1—C4—C5 of −81.78(5)°, 8.51(8)° and −171.06(8)°, respectively (Table 1). Two pyridine moieties are in the nearly *gauche* position, with the dihedral angle between the mean planes of both pyrimidine rings of 86.01(4)°; the corresponding angle is 78.13(5)° in the triclinic form (Cunha et al., 2007). Contrary to the triclinic form, the phenyl rings are nearly coplanar with the pyrimidine rings. The angle between the least-squares planes through N1—C6 and C21—C26 atoms is 3.54(4)°, and through N1′—C6′ and C21′—C26′ atoms is 3.13(6)°, whereas in the case of the triclinic form, the corresponding angles are 6.57(5)° and 9.29(5)°, respectively (Cunha et al., 2007). Additionally, two ethyl ester groups are twisted in relation to the pyrimidine rings, as shown by torsion angles around C5—C51 and C5′—C51′ bounds (Table 1).

The crystal structure analysis revealed different arrangement of molecules and intermolecular interactions between them to distinguish both polymorphs. There are no-direction-specific interactions between adjacent molecules in the triclinic form; the shortest distance H···*A* is longer than 2.7 Å (Cunha et al., 2007). In the case of the orthorhombic form, the molecules are linked by weak C—H···O interactions (Table 2), with C23 and C24′ phenyl atom as donors and ester atoms O51′($-x+1, y-1/2, -z+3/2$) and O51 ($x-1/2, y, -z+1/2$) as acceptors in these linkages (Fig. 4). There are also weak C—H···π interactions between molecules to complete the three-dimensional connectivity of the structure, but they are no considered in this paper.

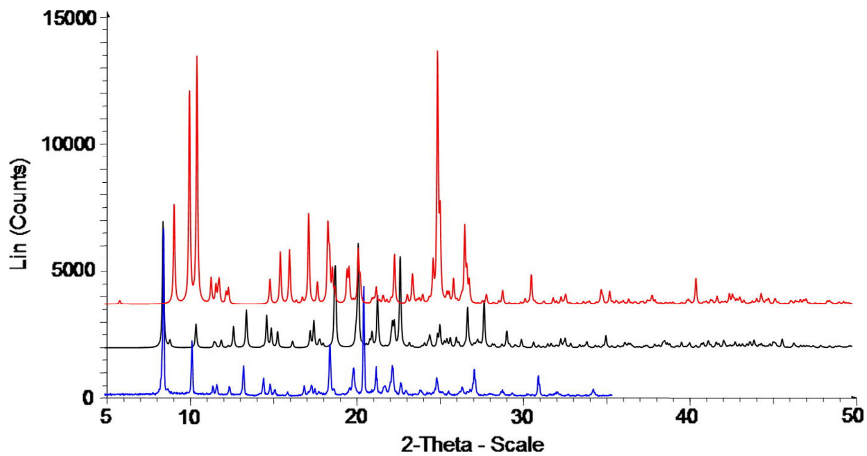

Figure 1 Simulated XRD pattern from the single crystal data of **DSMP** obtained for the triclinic (red) and orthorhombic (black) forms, and the experimental XRD patterns of the powdered crystals of the orthorhombic form (blue).

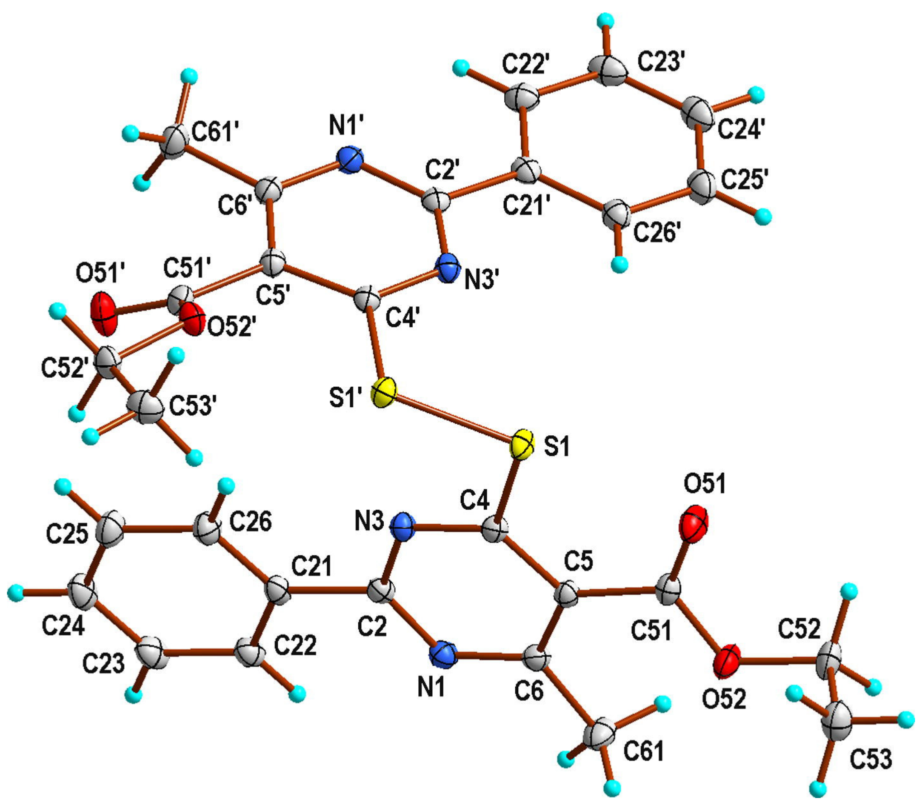

Figure 2 X-ray structure of the **DSMP** orthorhombic form, showing the atom-numbering scheme. Displacement ellipsoids are drawn at the 50% probability level. H atoms are shown as small spheres of arbitrary radii.

3.2. IR and Raman spectra

The PED data show that three types of vibrations could be identified for the studied compound. The normal modes, in which mainly one structural unit contributes to the vibration, form the first class of vibrations. The vibrations in which the separate CH_3, C_2H_5, C=O units participate belong to this type. The second type of normal modes constitutes of the skeleton vibrations activating mainly the benzene ϕ or pyrimidine θ rings. The normal modes originating from the coupled vibrations, both the skeleton and substituted groups, i.e. mixed modes, form the third type of vibrations. This classification has been used in Table 3 that lists the calculated and observed band wavenumbers together with their assignments to the respective normal modes.

Table 1 A comparsion of principal bond distances [Å], bond and torsion angles [°] of both polymorphic forms of **DSMP**.

	Orthorhombic form		Triclinic form[a]		Orthorhombic form		Triclinic form[a]
	Exp.	Calc.	Exp.		Exp.	Calc.	Exp.
Bond distance[*]							
S1—C4	1.7952 (11)	1.8045	1.7898 (18)	S1′—C4′	1.7927 (12)	1.8045	1.7865 (16)
C4—N3	1.3261 (13)	1.3181	1.322 (2)	C4′—N3′	1.3265 (13)	1.3180	1.325 (2)
C4—C5	1.4136 (14)	1.4169	1.411 (2)	C4′—C5′	1.4094 (14)	1.4082	1.406 (2)
N3—C2	1.3428 (13)	1.3362	1.337 (2)	N3′—C2′	1.3419 (14)	1.3367	1.337 (2)
C2—N1	1.3397 (13)	1.3377	1.334 (2)	C2′—N1′	1.3409 (14)	1.3375	1.339 (2)
C2—C21	1.4842 (14)	1.4793	1.476 (3)	C2′—C21′	1.4841 (14)	1.4810	1.478 (2)
N1—C6	1.3415 (14)	1.3327	1.339 (3)	N1′—C6′	1.3403 (14)	1.3328	1.336 (2)
C6—C5	1.4115 (14)	1.4131	1.404 (3)	C6′—C5′	1.4078 (15)	1.4075	1.401 (2)
C6—C61	1.5024 (15)	1.5053	1.505 (3)	C6′—C61′	1.5035 (15)	1.5032	1.506 (2)
C5—C51	1.4837 (14)	1.4766	1.482 (3)	C5′—C51′	1.4882 (15)	1.4870	1.488 (2)
C51—O51	1.2141 (13)	1.2155	1.198 (2)	C51′—O51′	1.2102 (14)	1.2094	1.190 (2)
C51—O52	1.3273 (13)	1.3434	1.324 (2)	C51′—O52′	1.3378 (14)	1.3448	1.319 (2)
O52—C52	1.4605 (14)	1.4527	1.455 (3)	O52′—C52′	1.4621 (13)	1.4512	1.465 (3)
C52—C53	1.5079 (18)	1.5167	1.494 (3)	C52′—C53′	1.5042 (17)	1.5123	1.468 (3)
C21—C26	1.3980 (15)	1.3994	1.382 (3)	C21′—C26′	1.3978 (15)	1.3994	1.381 (3)
C21—C22	1.3986 (14)	1.3994	1.396 (3)	C21′—C22′	1.4024 (15)	1.3990	1.386 (3)
C22—C23	1.3927 (16)	1.3873	1.380 (3)	C22′—C23′	1.3913 (16)	1.3874	1.380 (3)
C23—C24	1.3895 (17)	1.3923	1.366 (4)	C23′—C24′	1.3876 (18)	1.3917	1.369 (4)
C24—C25	1.3938 (16)	1.3918	1.375 (4)	C24′—C25′	1.3895 (18)	1.3918	1.366 (3)
C25—C26	1.3893 (15)	1.3873	1.378 (3)	C25′—C26′	1.3903 (15)	1.3873	1.385 (3)
S1—S1′	2.0473 (5)	2.0870	2.0389 (7)				
Bond angle[**]							
C4—S1—S1′	100.95 (4)	102.13	101.92 (6)	C4′—S1′—S1	102.31 (3)	103.96	104.94 (6)
N3—C4—S1	116.21 (8)	117.12	115.94 (12)	N3′—C4′—S1′	116.71 (8)	117.58	117.98 (12)
N3—C4—C5	122.29 (9)	121.79	122.74 (16)	N3′—C4′—C5′	121.82 (10)	121.83	122.82 (15)
C5—C4—S1	121.50 (8)	121.08	121.30 (14)	C5′—C4′—S1′	121.44 (8)	120.54	119.20 (12)
C4—N3—C2	116.99 (9)	118.34	117.07 (15)	C4′—N3′—C2′	117.47 (9)	118.15	116.56 (14)
N1—C2—N3	125.77 (9)	124.53	125.27 (18)	N1′—C2′—N3′	125.64 (10)	124.67	125.64 (16)
N1—C2—C21	117.36 (9)	117.96	118.09 (17)	N1′—C2′—C21′	117.85 (9)	117.93	117.14 (15)
N3—C2—C21	116.87 (9)	117.52	116.62 (16)	N3′—C2′—C21′	116.51 (9)	117.39	117.21 (15)
C2—N1—C6	117.74 (9)	118.45	118.07 (16)	C2′—N1′—C6′	117.16 (9)	118.05	117.70 (15)
N1—C6—C5	120.93 (9)	121.06	121.17 (17)	N1′—C6′—C5′	121.53 (9)	121.21	121.24 (16)
N1—C6—C61	113.72 (9)	114.33	113.55 (19)	N1′—C6′—C61′	115.19 (10)	115.78	114.64 (17)
C5—C6—C61	125.35 (10)	124.61	125.3 (2)	C5′—C6′—C61′	123.28 (10)	123.02	124.10 (18)
C6—C5—C4	116.28 (9)	115.81	115.63 (17)	C6′—C5′—C4′	116.33 (9)	116.08	115.95 (16)
C6—C5—C51	125.08 (9)	125.72	126.04 (17)	C6′—C5′—C51′	120.20 (9)	120.31	124.59 (15)
C4—C5—C51	118.63 (9)	118.47	118.32 (17)	C4′—C5′—C51′	123.39 (10)	123.52	119.42 (15)
O51—C51—O52	124.01 (10)	122.61	122.77 (19)	O51′—C51′—O52′	124.12 (10)	123.34	124.01 (18)
O51—C51—C5	121.87 (10)	122.38	122.67 (17)	O51′—C51′—C5′	124.25 (10)	124.67	122.91 (16)
O52—C51—C5	114.12 (9)	115.01	114.56 (18)	O52′—C51′—C5′	111.62 (9)	111.99	113.06 (17)
C51—O52—C52	117.03 (9)	116.46	116.14 (18)	C51′—O52′—C52′	116.12 (8)	116.11	117.38 (19)
O52—C52—C53	110.01 (10)	111.49	107.8 (2)	O52′—C52′—C53′	107.16 (9)	107.58	108.1 (2)
C26—C21—C22	119.57 (10)	119.09	118.6 (2)	C26′—C21′—C22′	119.44 (10)	119.19	118.70 (18)
C26—C21—C2	120.26 (9)	120.30	120.57 (17)	C26′—C21′—C2′	119.77 (10)	120.35	121.23 (16)
C22—C21—C2	120.17 (10)	120.61	120.8 (2)	C22′—C21′—C2′	120.78 (10)	120.46	120.07 (18)
C25—C26—C21	120.24 (10)	120.55	120.8 (2)	C23′—C22′—C21′	119.60 (11)	120.32	120.84 (19)
C26—C25—C24	119.94 (11)	119.97	120.0 (3)	C24′—C23′—C22′	120.69 (11)	120.18	120.0 (2)
C23—C24—C25	120.13 (11)	119.90	120.1 (2)	C23′—C24′—C25′	119.85 (11)	119.82	119.5 (2)
C24—C23—C22	120.13 (10)	120.24	120.5 (2)	C24′—C25′—C26′	120.07 (11)	120.21	121.2 (2)
C23—C22—C21	119.98 (10)	120.25	120.1 (2)	C25′—C26′—C21′	120.33 (11)	120.28	119.7 (2)
Torsion angle[***]							
S1′—S1—C4—N3	8.51 (8)	9.80	−10.21 (13)	S1—S1′—C4′—N3′	−16.47 (8)	−11.98	13.73 (13)
S1′—S1—C4—C5	−171.06 (8)	−171.17	171.49 (12)	S1—S1′—C4′—C5′	161.86 (7)	165.24	−165.29 (11)
C5—C4—N3—C2	0.56 (15)	0.13	0.3 (2)	C5′—C4′—N3′—C2′	−0.67 (14)	0.52	−2.3 (2)
S1—C4—N3—C2	−179.00 (7)	179.16	−177.96 (11)	S1′—C4′—N3′—C2′	177.66 (7)	177.71	178.69 (11)
C4—N3—C2—N1	−1.05 (15)	−1.55	1.7 (2)	C4′—N3′—C2′—N1′	2.26 (15)	−1.12	3.2 (2)
C4—N3—C2—C21	178.03 (9)	178.87	−179.75 (14)	C4′—N3′—C2′—C21′	−177.55 (9)	178.87	−175.37 (14)
N3—C2—N1—C6	1.35 (16)	1.41	−1.8 (3)	N3′—C2′—N1′—C6′	−1.90 (15)	0.27	−1.2 (3)
C21—C2—N1—C6	−177.72 (9)	−179.01	179.61 (15)	C21′—C2′—N1′—C6′	177.91 (9)	−179.71	177.36 (14)

(*continued on next page*)

Table 1 (*continued*)

	Orthorhombic form		Triclinic form[a]		Orthorhombic form		Triclinic form[a]
	Exp.	Calc.	Exp.		Exp.	Calc.	Exp.
C2—N1—C6—C5	−1.14 (15)	0.15	0.0 (3)	C2′—N1′—C6′—C5′	−0.05 (15)	1.15	−1.7 (2)
C2—N1—C6—C61	178.34 (10)	−179.27	178.97 (17)	C2′—N1′—C6′—C61′	179.58 (10)	−178.94	179.45 (16)
N1—C6—C5—C4	0.73 (15)	−1.38	1.7 (2)	N1′—C6′—C5′—C4′	1.40 (15)	−1.64	2.4 (2)
C61—C6—C5—C4	−178.70 (10)	177.97	−177.12 (18)	C61′—C6′—C5′—C4′	−178.20 (10)	178.46	−178.87 (16)
N1—C6—C5—C51	−177.85 (10)	179.31	−177.90 (16)	N1′—C6′—C5′—C51′	−175.53 (9)	−178.16	−175.11 (15)
C61—C6—C5—C51	2.73 (17)	−1.34	3.2 (3)	C61′—C6′—C5′—C51′	4.87 (16)	1.94	3.6 (3)
N3—C4—C5—C6	−0.43 (15)	1.25	−1.9 (2)	N3′—C4′—C5′—C6′	−1.03 (14)	0.78	−0.3 (2)
S1—C4—C5—C6	179.11 (8)	−177.75	176.27 (12)	S1′—C4′—C5′—C6′	−179.28 (7)	−176.32	178.68 (12)
N3—C4—C5—C51	178.24 (9)	−179.39	177.75 (15)	N3′—C4′—C5′—C51′	175.79 (9)	177.18	177.34 (15)
S1—C4—C5—C51	−2.22 (13)	1.62	−4.1 (2)	S1′—C4′—C5′—C51′	−2.45 (14)	0.08	−3.7 (2)
C6—C5—C51—O51	169.71 (11)	170.14	179.29 (18)	C6′—C5′—C51′—O51′	37.17 (16)	37.68	140.3 (2)
C4—C5—C51—O51	−8.84 (15)	−9.16	−0.3 (3)	C4′—C5′—C51′—O51′	−139.54 (12)	−138.57	−37.1 (3)
C6—C5—C51—O52	−10.25 (15)	−10.42	−0.1 (3)	C6′—C5′—C51′—O52′	−143.83 (10)	−142.11	−41.0 (2)
C4—C5—C51—O52	171.20 (9)	170.28	−179.74 (14)	C4′—C5′—C51′—O52′	39.46 (13)	41.64	141.56 (17)
O51—C51—O52—C52	−1.46 (16)	−0.41	2.4 (3)	O51′—C51′—O52′—C52′	2.91 (15)	4.06	−2.9 (3)
C5—C51—O52—C52	178.50 (9)	−179.84	−178.16 (15)	C5′—C51′—O52′—C52′	−176.09 (8)	−176.15	178.4 (2)
C51—O52—C52—C53	92.71 (12)	84.23	173.20 (17)	C51′—O52′—C52′—C53′	161.74 (9)	−179.06	−141.9 (2)
N1—C2—C21—C26	176.86 (10)	177.07	−174.24 (16)	N1′—C2′—C21′—C26′	−176.96 (9)	178.11	172.57 (16)
N3—C2—C21—C26	−2.30 (15)	−3.32	7.1 (2)	N3′—C2′—C21′—C26′	2.87 (14)	−1.88	−8.7 (2)
N1—C2—C21—C22	−2.87 (14)	−2.88	5.6 (3)	N1′—C2′—C21′—C22′	2.51 (14)	−1.79	−7.7 (2)
N3—C2—C21—C22	177.97 (9)	176.73	−173.10 (16)	N3′—C2′—C21′—C22′	−177.67 (9)	178.22	170.99 (17)
C22—C21—C26—C25	0.45 (16)	−0.14	−0.8 (3)	C22′—C21′—C26′—C25′	0.81 (15)	0.03	0.4 (3)
C2—C21—C26—C25	−179.28 (10)	179.91	179.05 (18)	C2′—C21′—C26′—C25′	−179.72 (10)	−179.88	−179.91 (18)
C21—C26—C25—C24	0.36 (18)	0.01	0.8 (3)	C21′—C26′—C25′—C24′	−0.33 (17)	−0.13	0.0 (3)
C26—C25—C24—C23	−1.04 (19)	0.08	−0.2 (4)	C26′—C25′—C24′—C23′	−0.23 (17)	0.09	−0.5 (4)
C25—C24—C23—C22	0.90 (18)	−0.05	−0.4 (4)	C25′—C24′—C23′—C22′	0.29 (17)	0.06	0.6 (4)
C24—C23—C22—C21	−0.09 (17)	−0.08	0.3 (4)	C24′—C23′—C22′—C21′	0.20 (16)	−0.16	−0.3 (4)
C26—C21—C22—C23	−0.59 (16)	0.17	0.2 (3)	C26′—C21′—C22′—C23′	−0.74 (15)	0.11	−0.2 (3)
C2—C21—C22—C23	179.15 (10)	−179.88	−179.60 (19)	C2′—C21′—C22′—C23′	179.80 (10)	−179.98	−179.9 (2)
C4—S1—S1′—C4′	−81.78 (5)	−77.85	75.99 (7)				

[a] Cunha et al. (2007).
[*] RMSD (root mean square deviation) for the *bond distances* = 0.009.
[**] RMSD for the *bond angles* = 0.67.
[***] RMSD for the *torsion angles* = 2.84.

3.2.1. Benzene (ϕ) ring vibrations

The vibrational characteristics of the benzene ring vibrations in its mono- and polysubstituted derivatives are well known (Lin-vien et al., 1991; Socrates, 2001; Varsányi and Szőke, 1969). In the studied compound, both benzene rings are substituted by polar chromophore – pyrimidine ring. Therefore, we expect appearance of the bands originating from vibrations of ten CH bonds and two benzene rings in the IR and Raman spectra (Fig. 5 and Table 3). For the latter bonds the characteristic vibrations are observed in the following ranges (Raman lines in parentheses): νCH: 3089 (3090), 3062 (3070, 3064), 3056 (3057, 3044), 3033 (3035) cm^{-1}; $\delta CH_\phi + \nu\phi$: 1600, 1586 (1599); $\delta CH_\phi + \nu\theta$: 1511, 1495 (1495) cm^{-1}; $\delta\phi + \delta\theta + \delta CH_\phi$: 1303, δCH_ϕ: 1172, 1161 (1166), 1083, 1061 (1081), δϕ: 1026 (1028), $\nu_s\phi$: 1002 (1001); γCH_ϕ: 986, 949, 938 (988), 851 (851); $\gamma\theta + \gamma CH_\phi$: 816 (816); $\gamma CH_\phi + \omega OCO$: 751, 745 (748), γCH_ϕ: 702, 696; $\delta\phi + \delta\theta$: 675, 670 (672); $\gamma\phi + \gamma CH_\phi + \gamma\theta$: 662, 654 (660), δϕ: 619 (619) cm^{-1}; $\gamma\phi + \delta C_\theta$—O—Et: 463; $\gamma\phi + \gamma C_\theta—CH_3 + \gamma C_\theta$—O—Et: 449 cm^{-1}. These bands fit well the literature data (Lin-vien et al., 1991; Socrates, 2001; Varsányi and Szőke, 1969). The wavenumbers observed in the spectra are described as benzene (ϕ) ring modes. It should be noted that the vibrations originating form the benzene ring vibrations produce the characteristic doublet contours due to the appearance of two benzene rings in the molecule. This is observed for the bands at about 1590, 1510, 1490, 1170, 1080, 1025, 1000, 990, 940, 850, 815, 780, 750, 700, 675, 660 and 620 cm^{-1}. Because the experimental wavenumbers fit well those calculated in the quantum chemical procedure it confirms that the used basis set and B3LYP functional have been chosen properly.

3.2.2. Methyl and ethyl groups vibrations

The ν_sCH_3, $\nu_{as}CH_3$ and $\nu_sCH_{3(Et)}$, $\nu_{as}CH_{3(Et)}$ vibrations corresponding to symmetric and asymmetric stretching modes are usually observed in the range between 3010 and 2950 cm^{-1} (Lin-vien et al., 1991; Socrates, 2001; Varsányi and Szőke, 1969). Our DFT calculations for the studied compound locate these modes for methyl $—CH_3$ and ethyl $—CH_2—CH_3$ groups at the following wavenumbers: $\nu_{as}CH_3 + \nu_{as}CH_2$: 3015, 3000, 2996, 2993, 2988, 2981, 2972, 2958 and $\nu_sCH_3 + \nu_sCH_2$: 2941, 2938, 2926, 2925 cm^{-1}. They agree very well with the experimental values found at 3014 (3011), 2993, 2982 (2981, 2976), 2959 (2959) for $\nu_{as}(CH_3) + \nu_{as}CH_2$ and at 2937

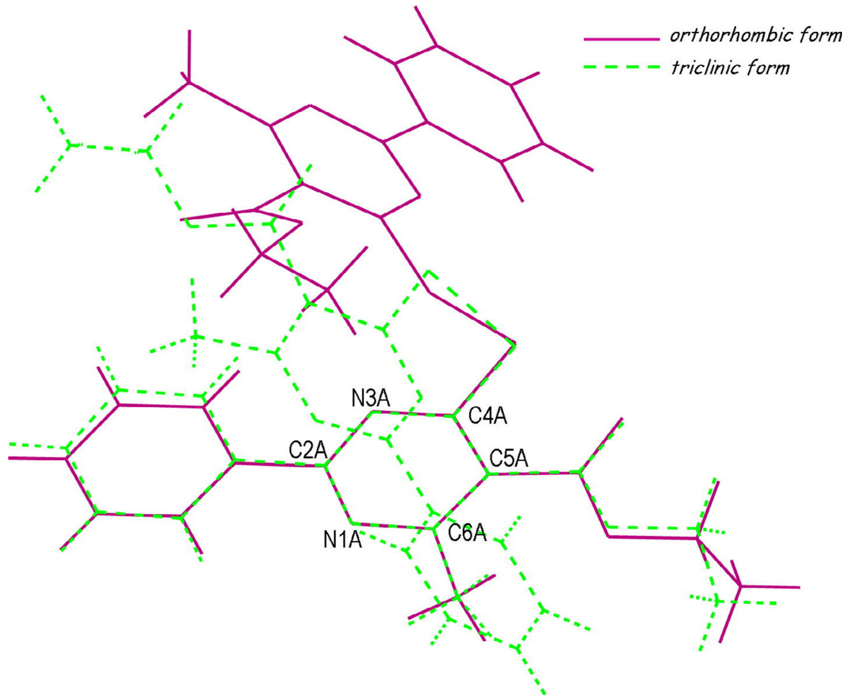

Figure 3 A comparison of structures: the orthorhombic (solid line) and triclinic (dashed line) forms of **DSMP**. The common reference points are N1, C2, C3, C4, C5 and C6 atoms of the pyrimidine ring.

Table 2 The short contacts geometry (Å, °) of the **DSMP** orthorhombic form.

D—H···*A*	*D*—H	H···*A*	*D*···*A*	*D*—H···*A*
C23—H23···O51′[i]	0.95	2.51	3.386 (2)	153
C24′—H24′···O51[ii]	0.95	2.34	3.273 (2)	167

Symmetry code: (i) $-x + 1, y - 1/2, -z + 3/2$; (ii) $x - 1/2, y, -z + 1/2$.

(2936), 2927, (2925) cm^{-1} for $\nu_s(CH_3)$ + $\nu_s CH_2$. The other bands in this region correspond to the vibrations of the ethyl group, and they are listed in Table 3.

The wavenumbers of bending vibrations of the methyl and ethyl groups are expected between 1500 and 1410 cm^{-1} (Lin-vien et al., 1991; Socrates, 2001; Varsányi and Szőke, 1969). Here for the studied compound $\delta_{as}CH_3$ vibrations of the methyl and ethyl groups contribute to the bands observed at 1475 (1475), 1467, 1455 (1452), 1449, 1440 (1440) and 1427 (1429, 1427) cm^{-1} and 1405, (1406), 1397 (1396), 1384 (1385), 1365 (1376), 1354 (1360) cm^{-1} for $\delta_s CH_3$. The symmetric bending vibrations of the methyl and ethyl groups also appear in the typical ranges and are observed at 1365 (1376) and 1354 (1360) cm^{-1} giving a great 90% contribution to the respective normal modes. The other bands involving the methyl and ethyl groups are observed in the following ranges: $\nu(C—C)_{Et}$: 1014, 872, 864 (872, 864) cm^{-1}; rocking ρEt and wagging ωCH_3: 1253, 1243, 1230 (1247, 1237), 1180 (1178), (1157), 1088 (1088), 783, 781, (775) cm^{-1}; τEt, γCH_3, and τCH_3: 1311, 1307 (1307), 1277 (1275), 807 (808), 564 (565), 302 (297), 239 (249, 236), 202 (218, 204), 180 (180) cm^{-1}.

3.2.3. Ester O=C—OEt group vibrations

Ester group is one of the substituents of the pyrimidine ring. The characteristic vibrations of this group *per analogiam* to other esters are observed in **DSMP** at following wavenumbers: νC=O: 1719, 1690 (1718, 1690) cm^{-1}; νOC—O: 1253, 1243, 1230 (1247, 1237); ν_{as}CO—C: 1088 (1088) cm^{-1}; δCOC: 807 (808) cm^{-1}; ωOCO: 751, 745 (748) and δ, ρ, γ bridge C_θ—O—Et: 463, 459, 449, 388 (389), 366, 350 (364, 351), 341 (341) cm^{-1}. The proposed assignment of these bands to the respective normal modes fits well with the literature data (Lin-vien et al., 1991; Socrates, 2001; Varsányi and Szőke, 1969) and the calculated in DFT procedure wavenumbers.

3.2.4. Pyrimidine (θ) ring vibrations

The vibrational characteristics of pyrimidine were described in several papers (Berezin et al., 2004; Centeno et al., 2006; Lin-vien et al., 1991; Tayyari et al., 2015). The forms of the normal modes as well as theoretical and experimental wavenumbers were presented in Howard et al. (2010); Shukla et al. (2014). The calculations were performed for the axial and equatorial conformations of the pyrimidine ring. The IR spectra of pyrimidine in the solid state (at 10 K) and in an argon matrix form were analyzed by Breda et al. (2006). The ^{1}H NMR and MS spectra of deuterium substituted pyrimidines form were analyzed by Milani-Nejad and Stidham, (1975). The possible conformations of the pyrimidine ring were considered using IR and NMR (Allenstein et al. 1976; Goto et al., 2013; Liu et al., 2014; Shkurko and Mamaev, 1987; Umemoto et al., 1984).

In the **DSMP** studied by us, the pyrimidine ring is four-substituted, bonded to methyl, ethyl, phenyl and disulfide groups. 6 × 3 = 18 normal modes should characterize the

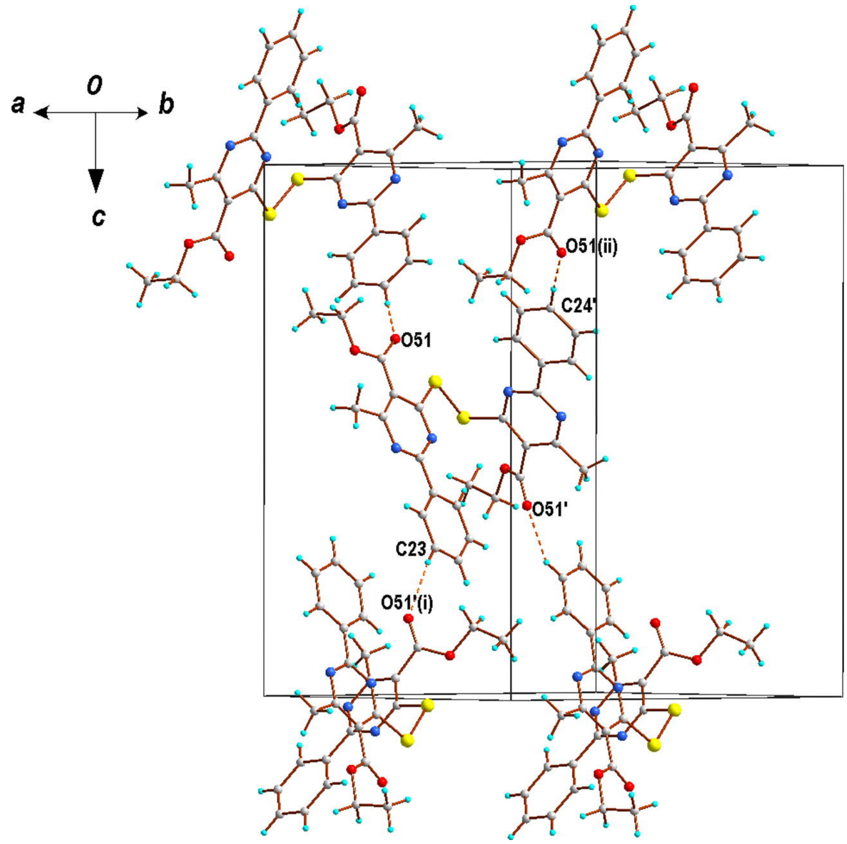

Figure 4 Part of the crystal structure of the **DSMP** orthorhombic form, showing C—H···O (orange dashed lines) interactions. Symmetry codes as in Table 2.

vibrations of the C_4N_2 ring. Their structure can be approximated by C_s symmetry and therefore all 18 ring vibrations are both IR and Raman active. In the monomeric structure these vibrations should be observed in the form of single bands, but for the dimer these lines can be split into two components due to the resonance effect originating from the in-phase and out-of-phase vibrations of two symmetric parts of this structure. The characteristic vibrations of the pyrimidine ring are observed at following wavenumbers (the bands of highest intensity are bold): stretching νθ: **1532**, **1511**, 1495, (**1527, 1495**), 1290 (1298, 1288), 923 (922) cm^{-1}; in-plane bending δθ: 1303, **1253**, **1243**, (1298, 1288), 1230 (1247, 1237), 1207, 1201 (1204, 1197), 1088 (1088), 923 (922), 576 (575) cm^{-1}; out-of-plane bending γθ: 816 (816), 675, 670 (672), 662, 654 (660), 564 (565) cm^{-1}; ρθ: 603 cm^{-1}. The vibration called a "breathing mode" is observed at 1002 cm^{-1} in the IR spectrum, and at 1001 cm^{-1} in the Raman spectrum. All these bands originate from the vibrations in which the quantum chemical DFT calculations predict a significant contribution of the internal coordinates of the pyrimidine ring. It should be noted, that the assignment of these experimental and theoretical wavenumbers to the respective ring vibrations is consistent with the results reported in the earlier works (Berezin et al., 2004; Breda et al., 2006; Centeno et al., 2006; Howard et al., 2010; Shukla et al., 2014; Tayyari et al., 2015).

3.2.5. C—S—S—C bridge group vibrations

Disulfide bridge is a group that influences the conformation of the compound studied most. According to the structural X-ray data reported here the length of the S—S bond equals to 2.0473(5) Å and those of S1—C4 and S1′—C4′ bonds 1.7952(11) and 1.7927(12) Å, respectively, i.e. there is a small difference between them. The angles between these bonds are C4—S1—S1′ 100.95(4)° and C4′—S1′—S1 102.31(3)° but the dihedral angle C4—S1—S1′—C4′ equals to −81.78(5)° (Table 1). Such a configuration of the disulfide bridge should be reflected in its vibrational behavior.

The assignment of the IR and Raman bands to the vibrations of the disulfide bridge is difficult due to their weak or medium intensity and their sensitivity to the adjacent environment. The vibrational characteristics of this bond were recognized mainly for the biological systems, e.g. amino acids and peptides (Nakamura et al., 1997; Parker, 1983; Podstawka et al., 2004; Young et al., 1995). It was found that the stretching νC—S vibration is observed in the form of a weak-to-medium band in the range 750–570 cm^{-1} but the νS—S vibration in the range 530–470 cm^{-1} (Socrates, 2001; Varsányi and Szőke, 1969). The geometry of the S—S bond strongly influences energy position and intensity of these bands. For instance, when the dihedral angle changes from 10°, through 30° and, at least, to 60°, the νS—S band changes from 509 to, 495 and 486 cm^{-1}, respectively (Parker, 1983). It was predicted that when the dihedral angle is close to 90° the

Table 3 Experimental and calculated wavenumbers (cm^{-1}), and assignments of the **DSMP** orthorhombic form.

No	Theoretical* GAS Phase/B3LYP/6-311G (2d,2p)			Experimental		PED	Assignment**
		IR Abs.	RS Int.	IR***	RS		
	(cm^{-1})	(%)					
1	3101	0	8			85 νCH_{ϕ}	νCH_{ϕ}
2	3086	1	11	3089 vw	3090 sh	83 νCH_{ϕ}	νCH_{ϕ}
3	3086	1	7			83 νCH_{ϕ}	νCH_{ϕ}
4	3084	1	5			82 νCH_{ϕ}	νCH_{ϕ}
5	3064	3	25	3062 w	3070 m	88 νCH_{ϕ}	νCH_{ϕ}
6	3060	4	31		3064 m	88 νCH_{ϕ}	νCH_{ϕ}
7	3054	2	18	3056 vw	3057 sh	88 νCH_{ϕ} + 10 $\nu\phi$	νCH_{ϕ}
8	3050	2	15			86 νCH_{ϕ} + 11 $\nu\phi$	νCH_{ϕ}
9	3040	0	9	3033 vw	3044 sh	88 νCH_{ϕ}	νCH_{ϕ}
10	3038	0	7		3035 vw	85 νCH_{ϕ}	
11	3026	1	6			96 $\nu_{as}CH_3$	$\nu_{as}CH_3$
12	3022	1	7			95 $\nu_{as}CH_3$	
13	3015	3	1	3014 vw	3011 w	44 $\nu_{as}CH_2$ + 39 $\nu_{as}CH_{3(Et)}$	$\nu_{as}CH_2$ + $\nu_{as}CH_{3(Et)}$
14	3000	5	2			56 $\nu_{as}CH_{3(Et)}$ + 28 $\nu_{as}CH_2$	
15	2996	1	8	2993 sh		43 $\nu_{as}CH_{3(Et)}$ + 30 $\nu_{as}CH_2$	$\nu_{as}CH_{3(Et)}$ + $\nu_{as}CH_2$
16	2993	1	8			94 $\nu_{as}CH_3$	$\nu_{as}CH_3$
17	2988	1	7	2982 m	2981 w	93 $\nu_{as}CH_3$	$\nu_{as}CH_3$
18	2988	4	14			77 $\nu_{as}CH_3$ + 9 $\nu_{as}CH_2$	$\nu_{as}CH_{3(Et)}$
19	2981	4	17		2976 w	64 $\nu_{as}CH_3$ + 16 $\nu_{as}CH_2$	$\nu_{as}CH_{3(Et)}$ + $\nu_{as}CH_2$
20	2972	0	10			48 $\nu_{as}CH_2$ + 32 $\nu_{as}CH_{3(Et)}$	$\nu_{as}CH_2$ + $\nu_{as}CH_{3(Et)}$
21	2958	3	13	2959 w	2959 w	59 ν_sCH_2 + 20 $\nu_{as}CH_{3(Et)}$	ν_sCH_2 + $\nu_{as}CH_{3(Et)}$
22	2941	1	25	2937 w	2936 sh	84 ν_sCH_3	ν_sCH_3
23	2940	2	13			87 ν_sCH_2	ν_sCH_2
24	2938	1	21			88 ν_sCH_3	ν_sCH_3
25	2926	2	23	2927 vw	2925 m	92 $\nu_sCH_{3(Et)}$	$\nu_sCH_{3(Et)}$
26	2925	3	25	2904 w		93 $\nu_sCH_{3(Et)}$	
				2866 vw	2892 vw		combination
					2865 vw		
27	1721	43	9	1719 vs	1718 m	63 νCO	$\nu C{=}O$
				1703 sh			
28	1688	39	23	1699 sh	1690 w	64 νCO + 18 $\delta_sCH_{2(Et)}$	$\nu C{=}O$
				1690 m	1686 sh		
				1665 sh			
29	1610	0	51	1600 w	1599 vs	42 $\nu\phi$ + 33 δCH_{ϕ}	$\nu\phi$ + δCH_{ϕ}
30	1609	1	44			43 $\nu\phi$ + 41 δCH_{ϕ}	
31	1591	0	0	1586 w		40 $\nu\phi$ + 38 δCH_{ϕ}	$\nu\phi$ + δCH_{ϕ}
32	1590	0	0			40 $\nu\phi$ + 39 δCH_{ϕ}	
33	1541	63	100	1562 sh	1559 sh	40 $\nu\theta$ + 28 δCH_3	$\nu\theta$ + $\delta_{as}CH_3$
				1550 sh	1551 sh		
					1543 sh		
34	1534	100	73	1532 vs	1537 sh	35 $\nu\theta$ + 26 δCH_3	$\nu\theta$ + $\delta_{as}CH_3$
					1527 m		

(continued on next page)

Table 3 (*continued*)

No	Theoretical[*] GAS Phase/B3LYP/6-311G (2d,2p)			Experimental		PED	Assignment[**]
		IR Abs.	RS Int.	IR[***]	RS		
	(cm^{-1})	(%)					
35	1508	22	2	1511 s		31 $\nu\theta$ + 18 δCH_{ϕ} + 13 δCH_3	$\nu\theta$ + δCH_{ϕ} + $\delta_s CH_3$
36	1501	14	17	1495 sh	1495 m	42 $\nu\phi$ + 17 $\nu\theta$ + 15 δCH_3	$\nu\phi$ + $\nu\theta$
37	1500	22	12			37 $\nu\phi$ + 17 $\nu\theta$ + 15 δCH_3	
38	1498	11	26			38 $\nu\phi$ + 15 $\nu\theta$ + 15 δCH_3	
39	1493	0	0			47 $\delta_s CH_2$ + 46 $\delta_{as} CH_{3(Et)}$	$\delta_s CH_2$ + $\delta_{as} CH_{3(Et)}$
40	1485	1	0	1475 vw	1475 vw	65 $\delta_{as} CH_{3(Et)}$ + 26 $\delta_s CH_2$	$\delta_{as} CH_{3(Et)}$ + $\delta_s CH_2$
41	1475	1	1			54 $\delta_{as} CH_{3(Et)}$ + 41 $\delta_s CH_2$	
42	1467	2	4	1467 vw		50 $\delta_s CH_2$ + 35 $\delta_{as} CH_{3(Et)}$	$\delta_s CH_2$ + $\delta_{as} CH_{3(Et)}$
43	1463	1	2			72 $\delta_{as} CH_{3(Et)}$	$\delta_{as} CH_{3(Et)}$
44	1463	2	4			67 $\delta_{as} CH_{3(Et)}$ + 28 $\delta_s CH_2$	$\delta_{as} CH_{3(Et)}$ + $\delta_s CH_2$
45	1460	1	1			71 $\delta_{as} CH_3$ + 10 δCH_{ϕ}	$\delta_{as} CH_3$
46	1460	1	1			58 $\delta_{as} CH_3$ + 18 δCH_{ϕ}	
47	1453	1	0	1455 vw	1452 w	33 $\nu\phi$ + 30 $\delta_{as} CH_3$ + 14 δCH_{ϕ}	$\nu\phi$ + $\delta_{as} CH_3$
48	1452	7	1			32 $\nu\phi$ + 26 δCH_3 + 13 $\nu\theta$	
49	1447	21	9	1449 vw	1440 vw	65 δCH_3	$\delta_{as} CH_3$
				1440 vw			
50	1444	23	7	1427 m	1429 w	70 δCH_3 + 10 $\nu\theta$	$\delta_{as} CH_3$
					1427 w		
51	1403	3	2	1405 vw	1406 sh	45 $\delta_s CH_{3(Et)}$ + 19 ωCH_2	$\delta_s CH_{3(Et)}$ + ωCH_2
52	1401	4	3			29 $\omega CH_{3(Et)}$ + 22 ωCH_2 + 11 $\delta\theta$ + 10 COO	$\omega CH_{3(Et)}$ + ωCH_2
53	1392	4	13	1397 vw	1396 w	28 ωCH_3 + 22 ωCH_2 + 14 $\delta\theta$	ωCH_3 + ωCH_2
54	1391	3	4			34 $\delta_s CH_{3(Et)}$ + 27 ωCH_2 + 11 $\delta\theta$	$\delta_s CH_{3(Et)}$ + ωCH_2
55	1389	3	2	1384 w	1385 w	43 $\delta_s CH_3$ + 15 $\delta_s CH_{3(Et)}$	$\delta_s CH_3$ + $\delta_s CH_{3(Et)}$
56	1387	2	2			35 $\delta_s CH_3$ + 27 $\delta_s CH_{3(Et)}$	
57	1376	9	11		1376 sh	28 ωCH_2 + 27 $\delta_s CH_{3(Et)}$ + 10 $\delta_s CH_3$	ωCH_2 + $\delta_s CH_{3(Et)}$
58	1371	8	14			33 ωCH_2 + 23 $\delta_s CH_{3(Et)}$ + 11 $\delta_s CH_3$	
59	1360	6	6	1365 m	1360 m	22 δCH_{ϕ} + 19 $\delta_s CH_3$ + 16 $\delta\theta$ + 13 ωCH_2	δCH_{ϕ} + $\delta_s CH_3$
60	1359	9	6	1354 sh		21 δCH_{ϕ} + 20 $\delta_s CH_3$ + 18 $\delta\theta$ + 11 ωCH_2	
61	1325	1	1			54 δCH_{ϕ} + 24 $\delta\phi$	δCH_{ϕ} + $\delta\phi$
62	1323	1	1			54 δCH_{ϕ} + 26 $\delta\phi$	
63	1308	3	1	1311 m	1307 m	77 ωCH_2	$\omega CH_{3(Et)}$
				1307 sh			
64	1298	2	15	1303 sh		23 $\nu\phi$ + 21 δCH_{ϕ} + 15 $\nu\theta$	$\nu\phi$ + δCH_{ϕ} + $\delta\theta$
65	1297	31	31	1290 w	1298 sh	31 $\nu\phi$ + 19 $\nu\theta$ + 12 $\nu_{as}\phi$—COO	$\nu\phi$ + $\nu\theta$ + $\nu_{as}\phi$—COO
66	1290	44	24		1288 sh	37 $\nu\phi$ + 20 $\nu_{as}\phi$—COO + 12 ωCH_2 + 11 $\nu\theta$	
67	1275	3	7	1277 w	1275 w	39 τCH_2 + 10 τCH_3 + 10 δCH_{ϕ}	τCH_2
68	1274	5	7			38 τCH_2 + 11 δCH_{ϕ} + 10 $\tau CH_{3(Et)}$ + 10 COO	τCH_2
69	1243	82	18	1253 vs	1247 w	37 ν_{as}CO—O + 17 $\nu\theta$ + 17 ωCH_3	ν_{as}CO—O + $\nu\theta$ + ωCH_3
				1243 m			
70	1241	34	5	1230 sh	1237 sh	20 ν_{as}CO—O + 13 ωCH_3 + 14 $\nu\theta$	ν_{as}CO—O + ωCH_3 + $\nu\theta$
71	1210	4	1	1207 w	1204 w	36 $\delta\theta$ + 13 ρCH_3 + 10 δCH_{ϕ} + 10 ν_{as}CO—O + 8 δC_{θ}—S	$\delta\theta$ + ρCH_3 + δCH_{ϕ} + ν_{as}CO—O + δC_{θ}—S

72	1203	28	3	1201 vw	1197 sh	$39\ \delta\theta + 11\ \rho CH_2 + 9\ \delta CH_\phi + 7\ \delta C_\theta{-}S{-}S$	$\delta\theta + \rho CH_2 + \delta CH_\phi + \delta C_\theta{-}S{-}S$
73	1177	10	1	1180 w	1178 w	$34\ \rho CH_{3(Et)} + 32\ \rho CH_2 + 13\ \delta CH_\phi$	$\rho CH_{3(Et)} + \rho CH_2$
74	1176	9	3	1172 w		$54\ \delta CH_\phi + 10\ \delta\phi$	δCH_ϕ
75	1175	4	3			$41\ \delta CH_\phi + 17\ \rho CH_{3(Et)} + 16\ \rho CH_2$	$\delta CH_\phi + \rho CH_{3(Et)} + \rho CH_2$
76	1159	0	1	1161 w	1166 w	$70\ \delta CH_\phi + 16\ \nu\phi$	δCH_ϕ
77	1159	0	1			$72\ \delta CH_\phi + 16\ \nu\phi$	
78	1156	1	0		1157 w	$44\ \rho CH_{3(Et)} + 34\ \rho CH_2 + 14\ \nu C_\theta{-}COO$	$\rho CH_{3(Et)} + \rho CH_2$
79	1120	9	4	1125 m	1124 w 1120 sh	$17\ \delta\phi + 15\ \delta C_\theta{-}COO + 14\ \delta\theta + 13\ \delta CH_\phi$	$\delta\phi + \delta C_\theta{-}COO + \delta\theta + \delta CH_\phi$
80	1118	8	1	1115 sh	1114 w	$46\ \delta O{-}CH_2{-}CH_3 + 13\ \delta\theta + 9\ \delta CH_\phi$	$\delta O{-}CH_2{-}CH_3 + \delta\theta + \delta CH_\phi$
81	1113	7	3			$45\ \delta O{-}CH_2{-}CH_3 + 11\ \delta CH_\phi + 8\ \delta\theta$	
82	1096	10	0			$40\ \omega CH_{3(Et)} + 28\ \rho O{-}Et$	$\omega CH_{3Et} + \rho O{-}Et$
83	1082	20	0	1088 m	1088 vw	$22\ \nu_{as}CO{-}C + 16\ \delta CH_\phi + 15\ \delta\theta + 10\ \delta\phi$	$\nu_{as}CO{-}C + \delta CH_\phi + \delta\theta + \text{breath}\ \theta$
84	1081	7	0	1083 m	1081 vw	$22\ \delta CH_\phi + 18\ \nu_{as}CO{-}C + 10\ \delta\theta + 9\ \delta\phi$	$\delta CH_\phi + \nu_{as}CO{-}C$
85	1080	1	0			$44\ \delta CH_\phi + 24\ \delta\phi$	$\delta CH_\phi + \delta\phi$
86	1079	12	0	1061 sh		$15\ \rho CH_3 + 14\ \nu CO{-}O + 13\ \delta\theta + 10\ \delta\phi + 8\ \rho CH_{3(Et)}$	$\rho CH_3 + \nu CO{-}O + \text{breath}\ \theta + \delta\phi$
87	1044	0	0			$55\ \omega CH_3 + 13\ \gamma\theta$	ωCH_3
88	1039	0	0			$54\ \omega CH_3 + 13\ \gamma\theta$	
89	1029	1	1	1026 w	1028 w	$29\ \delta CH_\phi + 23\ \delta\phi + 15\ \rho CH_3$	$\delta CH_\phi + \delta\phi + \rho CH_3$
90	1026	2	1			$34\ \delta\phi + 32\ \delta CH_\phi + 19\ \rho CH_3$	
91	1010	4	0	1014 m		$37\ \rho CH_3 + 11\ \delta\theta + 11\ \nu(C{-}C)_{Et} + 8\ \nu O{-}Et$	$\rho CH_3 + \delta\theta + \nu(C{-}C)_{Et}$
92	1009	6	0			$17\ \rho CH_3 + 15\ \nu(C{-}C)_{Et} + 12\ \delta\theta$	
93	1005	1	1			$28\ \omega CH_3 + 24\ \gamma CH_\phi$	$\omega CH_3 + \gamma CH_\phi$
94	1003	0	1			$55\ \gamma CH_\phi + 19\ \gamma\phi$	$\gamma CH_\phi + \gamma\phi$
95	1002	1	8	1002 w	1001 m	$49\ \gamma CH_\phi + 20\ \delta\phi + 10\ \nu\phi$	$\gamma CH_\phi + \text{breath}\ \phi$
96	1000	0	10			$25\ \gamma CH_\phi + 18\ \omega CH_3 + 16\ \delta\phi + 12\ \nu\phi$	$\gamma CH_\phi + \text{breath}\ \phi + \omega CH_3$
97	998	0	0			$69\ \gamma CH_\phi + 15\ \gamma\phi$	γCH_ϕ
98	991	2	1			$26\ \omega CH_3 + 18\ \nu O{-}Et + 16\ \delta\theta + 14\ \nu(C{-}C)_{Et}$	$\omega CH_3 + \nu O{-}Et + \nu(C{-}C)_{Et} + \text{breath}\ \theta$
99	988	0	0	986 vw	988 vw	$70\ \gamma CH_\phi + 10\ \gamma\phi$	γCH_ϕ
100	987	0	0			$71\ \gamma CH_\phi + 8\ \gamma\phi$	
101	950	0	0	949 vw		$60\ \gamma CH_\phi + 10\ \gamma\phi$	γCH_ϕ
102	950	0	0	938 vw		$60\ \gamma CH_\phi + 10\ \gamma\phi$	
103	916	1	1	923 w	922 w	$18\ \delta\theta + 16\ \nu C_\theta{-}CH_3 + 15\ \nu\phi + 8\ CH_\phi$	$\delta\theta + \nu C_\theta{-}CH_3 + \text{breath}\ \phi$
104	916	1	3			$21\ \delta\theta + 16\ \delta\phi + 15\ \nu C_\theta{-}CH_3 + 9\ \delta COO$	
105	862	2	1	872 w	872 sh	$30\ \rho CH_{3(Et)} + 15\ \omega CH_2 + 11\ \nu CO{-}Et$	$\rho(CH_3)_{Et} + \omega CH_2 + \nu CO{-}Et$
106	861	2	2	864 w	864 w	$20\ \rho CH_{3(Et)} + 18\ \omega CH_2 + 7\ \nu CO{-}Et$	
107	856	0	0	851 w	851 w	$74\ \gamma CH_\phi$	γCH_ϕ
108	853	0	0			$77\ \gamma CH_\phi$	
109	848	3	2			$22\ \delta COO + 17\ \delta\theta + 10\ \gamma CH_\phi + 9\ \delta O{-}Et + 6\ \nu C_\theta{-}S$	$\delta COO + \delta\theta + \gamma CH_\phi + \delta O{-}Et + \nu C_\theta{-}S$
110	842	2	2			$34\ \delta COO + 20\ \rho CH_2{-}CH_3 + 9\ \delta\theta$	$\delta COO + \rho CH_2{-}CH_3$
111	830	0	0			$25\ \gamma\theta + 20\ \gamma CH_\phi + 16\ \gamma\theta{-}\phi + 8\ \omega COO$	$\gamma\theta + \gamma CH_\phi + \gamma\theta{-}\phi + \omega COO$
112	827	0	0	816 w	816 w	$22\ \gamma\theta + 20\ \gamma CH_\phi + 17\ \gamma\theta{-}\phi + 9\ \rho CH_3$	$\gamma\theta + \gamma CH_\phi + \gamma\theta{-}\phi$
113	806	3	1	807 w	808 w	$25\ \delta COC + 12\ \tau CH_{3(Et)} + 12\ \gamma\theta + 8\ \tau CH_2$	$\delta COC + \tau CH_{3(Et)} + \gamma\theta$
114	802	10	1			$22\ \delta COC + 11\ \tau CH_{3(Et)} + 11\ \delta\theta + 10\ \tau CH_2$	$\delta COC + \tau CH_{3(Et)} + \delta\theta$
115	800	1	0			$31\ \rho CH_2 + 24\ \rho CH_{3(Et)} + 10\ \omega COO + 8\ \gamma CH_\phi$	$\rho CH_2 + \rho CH_{3(Et)} + \omega COO$
116	791	2	0			$20\ \gamma CH_\phi + 21\ \omega COO + 9\ \gamma\theta + 8\ \gamma\phi$	$\gamma CH_\phi + \omega COO$
117	782	4	0	783 m 781 m		$20\ \gamma CH_\phi + 15\ \omega COO + 8\ \gamma\phi$	$\gamma CH_\phi + \omega COO$

(*continued on next page*)

Table 3 (*continued*)

No	Theoretical* GAS Phase/B3LYP/6-311G (2d,2p)			Experimental		PED	Assignment**
		IR Abs.	RS Int.	IR***	RS		
	(cm^{-1})	(%)					
118	766	0	1		775 vw	37 ρCH_2 + 27 $\rho CH_{3(Et)}$ + 10 ωCOO	ρCH_2 + ρCH_3
119	750	1	0	751 w	748 vw	22 γCH_ϕ + 21 ωCOO + 16 $\gamma\theta$ + 15 $\gamma\phi$	γCH_ϕ + $\gamma\phi$ + $\gamma\theta$ + ωCOO
120	749	2	0	745 w		27 γCH_ϕ + 19 $\gamma\theta$ + 18 $\gamma\phi$ + 18 ωCOO	
121	697	5	0	702 m		47 γCH_ϕ + 22 $\gamma\phi$	γCH_ϕ + $\gamma\phi$
122	697	6	0	696 m		45 γCH_ϕ + 28 $\gamma\phi$	
123	679	1	0	675 w	672 vw	20 $\delta\phi$ + 17 γCH_ϕ + 13 $\gamma\theta$	$\delta\phi$ + γCH_ϕ + $\gamma\theta$
124	674	1	0	670 w		22 $\delta\phi$ + 15 γCH_ϕ + 12 $\gamma\theta$ + 10 ρCH_2 + 10 δCOO	$\delta\phi$ + γCH_ϕ + $\gamma\theta$
125	667	1	0	662 w	660 vw	18 $\gamma\phi$ + 16 $\gamma\theta$ + 16 γCH_ϕ + 7 ωCH_3	$\gamma\phi$ + $\gamma\theta$ + γCH_ϕ
126	660	1	0	654 w		15 $\gamma\theta$ + 12 $\gamma\phi$ + 9 ωCH_3 + 8 γCH_ϕ	
127	624	0	1	619 vw	619 m	60 $\delta\phi$	$\delta\phi$
128	623	0	1			66 $\delta\phi$	
129	606	1	0	603 w		14 δC_θ—S—S + 14 δC_θ—CH_3 + 14 $\tau\theta$ + 14 $\tau\phi$ + 11 δCOO	δC_θ—S—S + δC_θ—CH_3
130	593	0	1	594 vw	593 w	16 δC_θ—S—S + 15 δC_θ—CH_3 + 14 δCOO + 11 $\tau\theta$	
131	582	0	0	587 sh		27 γCH_3 + 19 $\gamma\theta$ + 13 δCOO + 10 δC_θ—S	γCH_3 + $\gamma\theta$
132	575	0	2	576 w	575 m	27 $\delta\theta$ + 21 γCH_3 + 11 δC_θ—S + 8 δCOO	$\delta\theta$ + γC_θ—CH_3 + δC_θ—S
133	574	1	0			33 $\delta\theta$ + 22 γCH_3 + 11 δC_θ—S + 7 δCOO	
134	568	1	1	564 vw	565 w	25 $\gamma\theta$ + 21 γCH_3 + 13 γC_θ—S	$\gamma\theta$ + γCH_3 + γC_θ—S
135	504	0	2	521 vw	520 m	20 νS—S + 11 $\delta\theta$ + 11 δCOO	νS—S + $\delta\theta$ + δCOO
136	487	0	1	499 vw	499 w	19 $\gamma\phi$ + 12 γCH_ϕ + 10 $\gamma\theta$ + 11 νS—S	$\gamma\phi$ + γCH_ϕ + νS—S + δCOO
				486 vw	487 w		
137	473	1	2		473 w	18 $\gamma\phi$ + 16 γCH_ϕ + 11 δCOO + 10 νS—S	
138	470	0	1			22 $\gamma\phi$ + 16 γCH_ϕ + 13 $\delta\theta$ + 11 ρC_θ—CH_3	$\gamma\phi$ + γCH_ϕ + $\delta\theta$ + ρC_θ—CH_3
139	469	0	0	463 vw		22 γCH_ϕ + 22 $\gamma\phi$ + 11 δO—CH_2—CH_3 + 9 $\delta\theta$	γCH_ϕ + $\gamma\phi$ + δO—CH_2—CH_3
140	453	1	0	459 vw		22 δO—CH_2—CH_3 + 19 δC_θ—COO + 14 $\gamma\phi$ + 12 γCH_ϕ	δO—CH_2—CH_3 + δC_θ—COO + $\gamma\phi$ + γCH_ϕ
141	442	0	0	449 vw		18 $\gamma\phi$ + 16 γCH_ϕ + 13 δC_θ—COO + 10 δO—CH_2—CH_3 + 9 C_θ—CH_3	$\gamma\phi$ + γCH_ϕ + δC_θ—COO + δO—CH_2—CH_3
142	409	0	0			48 $\gamma\phi$ + 44 γCH_ϕ	$\gamma\phi$ + γCH_ϕ
143	409	0	0			50 $\gamma\phi$ + 44 γCH_ϕ	
144	380	1	0	388 w	389 w	21 ρCOOEt + 21 δO—Et + 8 $\delta\theta$—ϕ	ρCO—O—Et + δO—Et + $\delta\theta$—ϕ
145	376	1	0			28 ρCOOEt + 15 CH_{Et} + 10 δC_θ—S	δC_θ—S + ρCO—O—Et
146	365	4	1	366 w	364 w	23 ρCOOEt + 20 $\gamma(CH_3)_{Et}$ + 11 νC_θ—S	ρCOOEt + $\gamma(CH_3)_{Et}$ + νC_θ—S
147	345	1	0	350 w	351 m	24 ρEt + 20 δCOOEt	ρEt + δCOOEt
148	344	0	0			24 ρEt + 31 δCOOEt + 7 δC_θ—ϕ	ρEt + δCOOEt
149	337	2	0	341 vw	341 sh	20 ρEt + 25 δCOOEt + 6 ρCH_3	ρEt + δCOOEt
150	333	0	0			15 δC_θ—S + 13 $\gamma\theta$ + 12 ρCH_3 + 12 ρEt + 10 $\tau\phi$ + 9 δCOOEt	δC_θ—S + ρCH_3 + $\gamma\theta$ + ρEt
151	288	1	0	302 w	297 w	15 ρCH_3 + 12 ρEt + 11 $\tau\theta$ + 10 γCH_ϕ	ρCH_3 + ρEt + δC_θ—COO
152	285	0	0			18 ρCH_3 + 16 δC_θ—COO + 13 $\tau\theta$ + 12 γCH_ϕ	
153	281	1	0			24 τEt + 30 δC_θ—COO + 12 $\gamma\theta$	τEt + δC_θ—COO
154	263	1	0			38 τEt + 24 δC_θ—COOEt	τEt + δC_θ—COOEt
155	247	0	0	239 vw	249 sh	70 τEt	τEt
156	239	0	0			40 τEt + 19 δC_θ—COOEt	τEt + δC_θ—COOEt
157	235	2	0		236 m	40 τEt + 13 δC_θ—COOEt	τEt + δC_θ—COOEt

158	222	0	0			58 τEt	τEt
159	216	0	0		218 w	18 τCH_3 + 17 $\gamma\theta$—ϕ + 10 δC_θ—S + 10 γCH_ϕ	τCH_3 + $\gamma\theta$—ϕ + δC_θ—S + skeleton
160	212	0	0			34 τCH_3 + 17 $\tau\theta$—ϕ + 7 δC_θ—S	
161	211	0	0	202 vw	204 vw	24 γCH_3 + 18 $\gamma\theta$—ϕ + 12 τEt	γCH_3 + $\gamma\theta$—ϕ + τEt
162	200	0	0			28 τCH_3 + 22 τEt	τCH_3 + τEt
163	191	0	0			54 τCH_3	τCH_3
164	180	1	0	180 vw	180 sh	61 τEt + 8 $\gamma\theta$—ϕ	τEt
165	169	0	0		169 w	28 ρEt + 14 $\tau\theta$—ϕ + 13 γC_θ—S + 8 γCH_3	ρEt + $\tau\theta$—ϕ + γC_θ—S
166	165	0	0		162 sh	31 ρEt + 14 $\gamma\theta$—ϕ + 13 γCH_3 + 12 γC_θ—S	ρEt + $\gamma\theta$—ϕ + γCH_3 + γC_θ—S
167	135	0	0		139 sh	83 τCH_3	τCH_3
168	128	0	0			44 τEt + 15 γCH_3 + 10 γS—θ	τEt + γCH_3
169	118	0	0			44 τEt + 9 γCH_3 + 9 γS—θ	τEt
170	111	0	0		112 m	38 τCOO + 13 $\tau\theta$—ϕ + 10 γS—θ + 8 γEt	τCOO + $\tau\theta$—ϕ + τS—θ
171	96	0	0		98 sh	26 $\gamma\theta$—ϕ + 13 $\tau\phi$ + 12 γCH_3 + 8 τS—θ	$\tau\theta$—ϕ + $\tau\phi$ + γCH_3 + skeleton
172	87	0	0			38 $\tau\theta$—COOEt + 20 γCH_3 + 14 $\tau\theta$—ϕ	$\tau\theta$—COOEt + γCH_3 + $\tau\theta$—ϕ
173	83	0	0			31 $\tau\theta$—COOEt + 23 $\tau\theta$—ϕ + 11 γCH_3	
174	77	0	0			43 $\rho\theta$—COOEt + 14 γCH_3 + 11 $\gamma\theta$—ϕ	$\rho\theta$—COOEt + γCH_3 + $\gamma\theta$—ϕ
175	73	0	0			55 $\tau\theta$—COOEt + 14 $\gamma\theta$—ϕ	$\tau\theta$—COOEt + $\gamma\theta$—ϕ + skeleton
176	68	0	0			45 $\tau\theta$—COOEt + 12 γCH_3 + 11 $\gamma\theta$—ϕ	
177	64	0	0			27 $\tau\theta$—COO + 18 τEt + 11 γCH_3	flapping θ—ϕ + $\tau\theta$—COO + τEt
178	49	0	1			52 $\tau\theta$—ϕ + 14 $\tau\theta$—COO + 12 γCH_3	$\tau\theta$—ϕ + $\tau\theta$—COO + γCH_3 + skeleton
179	39	0	0			40 $\tau\theta$—COO + 24 $\tau\theta$—ϕ + 13 γCH_3	$\tau\theta$—COO + $\tau\theta$—ϕ + γCH_3 + skeleton
180	38	0	0			36 $\tau\theta$—COO + 24 $\tau\theta$—ϕ + 13 γCH_3	
181	32	0	0			37 $\tau\theta$—COO + 26 $\tau\theta$—ϕ	$\tau\theta$—COO + $\tau\theta$—ϕ + skeleton
182	25	0	0			40 $\gamma\theta$—COOEt + 20 γCH_3 + 10 $\gamma\theta$—ϕ	$\gamma\theta$—COOEt + γCH_3 + $\gamma\theta$—ϕ
183	24	0	0			34 γCH_3 + 17 $\tau\theta$—COO + 16 $\tau\theta$—ϕ	γCH_3 + $\tau\theta$—COO + $\tau\theta$—ϕ
184	20	0	1			27 τS—θ + 26 $\tau\theta$—ϕ + 23 γCH_3 + 10 $\tau\theta$—COO	τS—θ + $\tau\theta$—ϕ + γCH_3 + skeleton
185	12	0	1			28 γCH_3 + 28 $\gamma\theta$—COO + 16 τS—θ + 11 $\gamma\theta$—ϕ	γCH_3 + $\gamma\theta$—COO + τS—θ + skeleton
186	11	0	1			26 γCH_3 + 19 $\gamma\theta$—COO + 14 τS—θ + 11 $\gamma\theta$—ϕ	

Abbreviations used:

* Scaling factor: f_{sc} = 0.93 (3600–2500 cm^{-1}), f_{sc} = 0.98 (2499–0 cm^{-1}).

** ν – in-plane stretching vibrations; δ – in-plane bending vibrations; γ – out-of-plane bending vibrations; ρ – rocking vibrations; ω – wagging vibrations; τ – torsional vibrations; ϕ – benzene ring; θ – pyrimidine ring; Et – ethyl group; skeleton – complex vibrations of the whole θ unit and its substituents;

*** IR spectrum was measured in KBr pellet.

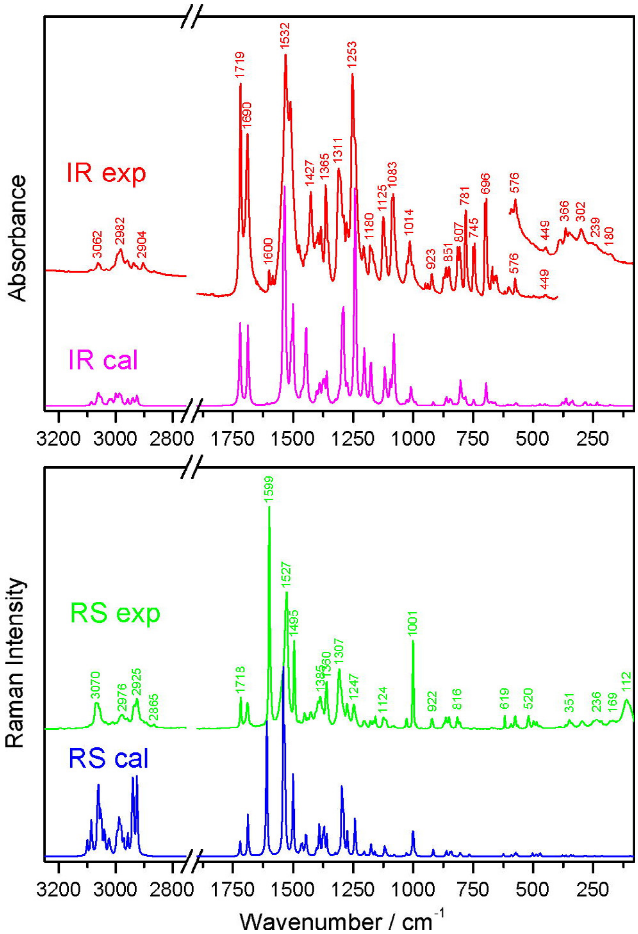

Figure 5 Experimental and calculated IR (top) and Raman (below) spectra of **DSMP** in the 3250–80 cm^{-1} range. IR spectrum was measured in KBr pellet.

wavenumber of this band is observed at about 505 cm^{-1}. These trends can be taken into account in the analysis of the disulfide bond vibrations in the **DSMP** studied by us.

The performed DFT calculations in this work place the vibrations of the C—S—S—C core in the range 525–470 cm^{-1} for the νS—S stretching mode and 370–360 cm^{-1} for the νC—S normal modes (Table 3 and Fig. S1 (Supplementary Data)). The DFT calculations locate the latter vibration at 365 cm^{-1} in the form of a single band because the geometry optimization approximates the molecule as symmetrical having the identical C—S bonds in the disulfide bridge. Both IR and Raman spectra exhibit in this range the single band at 366 cm^{-1} for the IR and at 364 cm^{-1} for the Raman spectra. This agrees with the X-ray data for which both C—S bonds have nearly the same bond lengths, 1.7952(11) and 1.7927(12) Å, i.e. these values are in the error limit. Besides, the PED calculations exhibit a small contribution of these internal coordinates also to a few other normal modes ν_{129}, ν_{130} and ν_{132}–ν_{134}, e.g. at about 610–590 and 580–560 cm^{-1}.

It should be noted that the intensity of the Raman band at 520 cm^{-1}, corresponding to the νS—S mode, is significantly greater than its IR counterpart at 521 cm^{-1}. This agrees with the X-ray structure of the studied compound.

The PED calculations locate in plane bending δC_0SS vibrations in the range 220–210 cm^{-1}, where the Raman line at 218 cm^{-1} is observed. The respective out-of-plane vibrations of these bonds are observed in the ranges 205–180 and 170–160 cm^{-1} (ν_{162}, ν_{164}–ν_{166}). The whole skeleton τ-vibrations, in which the C—S—S—C bridge also participates are located in the DFT calculations in the ranges 120–100, 65–40 and 20–10 cm^{-1}. The proposed in this work assignment of the bands to the respective normal modes in great outline agrees with that reported by Romani et al. (2015); small differences appear for the ν(C—S) vibrations that are observed in the spectra obtained by us at lower wavenumbers due to longer bond lengths in studied compound.

4. Conclusion

N_2C_4—S—S—C_4N_2 skeleton is an important component of several heterocyclic compounds and has a pharmaceutical and biological importance. The disulfide bridge coupling two pyrimidine rings is the characteristic unit of such compounds and the vibrational characteristics of this system can be used as a diagnostic tool for identification of these pharmaceuticals. In this work a discrimination procedure of characteristic for these compound bands from other lines appearing in the IR and Raman spectra has been proposed. Such an approach connects the theoretical considerations based on the quantum chemical calculations and the mathematical fitting of the theoretical and experimental spectra to assign the most characteristic lines to the considered skeleton. On that basis it was stated that the vibrations corresponding to the N_2C_4—S—S—C_4N_2 system contain a sequence of IR or Raman bands corresponding to the vibrations of the disulfide bridge. They are observed at about 603, 594, 587, 576, 564, 521, 499, 486, 366, 218, 202 cm^{-1} in the IR spectrum and at 593, 575, 565, 520, 499, 487, 473, 364, 351, 218 and 204 cm^{-1} in the Raman spectrum. Two stretching vibrations: ν(S—S) and ν(C—S) observed in the ranges 525–520 cm^{-1} and 605–575 cm^{-1}, respectively, are of the most valuable diagnostic importance. The appearance of these bands in the spectra of pharmaceuticals confirms the presence of this skeleton in such and similar substances.

Also other lines can be used as a diagnostic tool for identification of the pyrimidine ring in such pharmaceuticals. These are the bands observed at 1532, 1511, 1253, 1243 and 923 cm^{-1} in the IR spectrum, and at 1527, 922 and 575 cm^{-1} in the Raman spectrum.

Here the presented structural and spectroscopic data on diethyl 4 ,4′-disulfanediylbis(6-methyl-2-phenylpyrimidine-5-carboxylate) will be used in the future in the analysis of the interdependence between these properties and biological activity of similar compounds. In our earlier work seventeen newly obtained pyrimidine derivatives were tested microbiologically on 9 bacterial strains and one fungal strain (Cieplik et al., 2015). Some of the obtained compounds showed high antibacterial activity. Pyrimidine with multiple sulfide bridge showed interesting microbiological activity which was also affected by the functional group in position 5 of pyrimidine ring. The studies of the spectroscopic and structural properties of other such compounds will be continued in future.

Appendix A. Supplementary material

Supplementary data associated with this article can be found, in the online version, at Complete crystallographic data for the structural analysis have been deposited with the Cambridge Crystallographic Data Centre; CCDC reference number 1418446. These data can be obtained free of charge via www.ccdc.cam.ac.uk/conts/retrieving.html (or from the Cambridge Crystallographic Data Centre, 12 Union Road, Cambridge CB2 1EZ, UK; fax: (+44) 1223 336033; e-mail: deposit@ccdc.cam.ac.uk).http://dx.doi.org/10.1016/j.arabjc.2016.03.004.

References

Allenstein, E., Podszun, W., Kiemle, P., Mauk, H.-J., Schlipf, E., Weidlein, J., 1976. Die schwingungsspektren methylsubstituierter pyrimidine und s-triazine. Spectrochim. Acta A 32, 777–785.

Becke, A.D., 1996. Density-functional thermochemistry. IV. A new dynamical correlation functional and implications for exact-exchange mixing. J. Chem. Phys. 104, 1040–1046.

Berezin, K.V., Nechaev, V.V., El'kin, P.M., 2004. Anharmonic analysis of the vibrational states of pyrimidine by the density functional method. Opt. Spectrosc. 97, 210–220.

Brandenburg, K., 2005. DIAMOND, Ver. 3.0d, Crystal Impact GbR, Bonn, Germany.

Breda, S., Reva, I.D., Lapinski, L., Nowak, M.J., Fausto, R., 2006. Infrared spectra of pyrazine, pyrimidine and pyridazine in solid argon. J. Mol. Struct. 786, 193–206, and references therein.

Centeno, S.P., López-Tocón, I., Arenas, J.F., Soto, J., Otero, J.C., 2006. Selection rules of the charge transfer mechanism of surface-enhanced Raman scattering: the effect of the adsorption on the relative intensities of pyrimidine bonded to silver nanoclusters. J. Phys. Chem. B 110, 14916–14922.

Cieplik, J., Stolarczyk, M., Pluta, J., Gubrynowicz, O., Bryndal, I., Lis, T., Mikulewicz, M., 2015. Synthesis and antibacterial properties of pyrimidine derivatives. Acta Pol. Pharm. 72, 53–64.

Cocco, M.T., Congiu, C., Onnis, V., 1995. New thioxopyrimidines. Synthesis and evaluation for antimicrobial activity. Farmaco 50, 73–76.

Cocco, M.T., Congiu, C., Onnis, V., Piras, R., 2001. Synthesis and antitumor evaluation of 6-thioxo-, 6-oxo- and 2,4-dioxopyrimidine derivatives. Farmaco 56, 741–748.

Cunha, S., Bastos, R.M., Silva, P.O., Nobre Costa, G.A., Vencato, I., Luriucci, C., Napolitano, H.B., Oliveira, C.M.A., Kato, L., Silva, C.C., Menezes, D., Vannier-Santos, M.A.S., 2007. Synthesis and structural studies of 4-thioxopyrimidines with antimicrobial activities. Monatsh. Chem. 138, 111–119.

Frisch, M.J., Trucks, G.W., Schlegel, H.B., Scuseria, G.E., Robb, M. A., Cheeseman, J.R., Montgomery, J.A. Jr., Vreven, T., Kudin, K. N., Burant, J.C., Millam, J.M., Iyengar, S.S., Tomasi, J., Barone, V., Mennucci, B., Cossi, M., Scalmani, G., Rega, N., Petersson, G. A., Nakatsuji, H., Hada, M., Ehara, M., Toyota, K., Fukuda, R., Hasegawa, J., Ishida, M., Nakajima, T., Honda, Y., Kitao, O., Nakai, H., Klene, M., Li, X., Knox, J.E., Hratchian, H.P., Cross, J. B., Adamo, C., Jaramillo, J., Gomperts, R., Stratmann, R.E., Yazyev, O., Austin, A.J., Cammi, R., Pomelli, C., Ochterski, J.W., Ayala, P.Y., Morokuma, K., Voth, G.A., Salvador, P., Dannenberg, J.J., Zakrzewski, V.G., Dapprich, S., Daniels, A.D., Strain, M.C., Farkas, O., Malick, D.K., Rabuck, A.D., Raghavachari, K., Foresman, J.B., Ortiz, J.V., Cui, Q., Baboul, A.G., Clifford, S., Cioslowski, J., Stefanov, B.B., Liu, G., Liashenko, A., Piskorz, P., Komaromi, I., Martin, R.L., Fox, D.J., Keith, T., Al-Laham, M. A., Peng, C.Y., Nanayakkara, A., Challacombe, M., Gill, P.M.W., Johnson, B., Chen, W., Wong, M.W., Gonzalez, C., Pople J.A., 2003. Gaussian 03, Revision A.1, Gaussian Inc, Pittsburgh, PA.

Goto, T., Shiina, A., Yoshino, T., Mizukami, K., Hirahara, K., Suzuki, O., Sogawa, Y., Takahashi, T., Mikkaichi, T., Nakao, N., Takahashi, M., Hasegawa, M., Sasaki, S., 2013. Synthesis and biological evaluation of 5-carbamoyl-2-phenylpyrimidine derivatives as novel and potent PDE4 inhibitors. Bioorg. Med. Chem. 21, 7025–7037.

Howard, A.A., Tschumper, G.S., Hammer, N.I., 2010. Effects of hydrogen bonding on vibrational normal modes of pyrimidine. J. Phys. Chem. A 114, 6803–6810.

Krishnan, R., Binkley, J.S., Seeger, R., Pople, J.A., 1980. Self-consistent molecular orbital methods. XX. A basis set for correlated wave functions. J. Chem. Phys. 72, 650–654.

Li, S., Chen, J.M., Lu, T.B., 2014. Synthon polymorphs of 1: 1 co-crystal of 5-fluorouracil and 4-hydroxybenzoic acid: their relative stability and solvent polarity dependence of grinding outcomes. CrystEngCommun 16, 6450–6458.

Lin-vien, D., Cothup, N.B., Fateley, W.G., Graselli, J.G., 1991. The Handbook of Infrared and Raman Characteristic Frequencies of Organic Molecules. Academic Press, Boston.

Liu, M., Sun, X., Zhang, J., 2014. Synthesis and characterization of a series of novel 2-Schiff base-substituted phenyl pyrimidine. Arab. J. Chem., Corrected Proofs, (in press) (http://dx.doi.org/10.1016/j.arabjc.2014.11.053).

Lee, C., Yang, W., Parr, R.G., 1988. Development of the Colle–Salvetti correlation-energy formula into a functional of the electron density. Phys. Rev. B 37, 785–789.

Macrae, C.F., Edgington, P.R., McCabe, P., Pidcock, E., Shields, G.P., Taylor, R., Towler, M., van de Streek, J., 2006. Mercury: visualization and analysis of crystal structures. J. Appl. Cryst. 39, 453–457.

McLean, A.D., Chendler, G.S., 1980. Contracted Gaussian basis sets for molecular calculations. I. Second row atoms, Z = 11–18. J. Chem. Phys. 72, 5639–5648.

Michalska, D., 2002. RAINT (Raman Intensities) – a Computer Program for Calculation of Raman Intensities from the Gaussian Outputs. Wrocław University of Technology, Wrocław.

Michalska, D., Wysokiński, R., 2005. The prediction of Raman spectra of platinum(II) anticancer drugs by density functional theory. Chem. Phys. Lett. 403, 211–217, and references therein.

Milani-Nejad, F., Stidham, H.D., 1975. Spectra of C2v deuterium substituted pyrimidines. Spectrochim. Acta A 31, 1433–1453.

Nakamura, K., Era, S., Ozaki, Y., Sogami, M., Hayashi, T., Murakami, M., 1997. Conformational changes in seventeen cystine disulfide bridges of bovine serum albumin proved by Raman spectroscopy. FEBS Lett. 417, 375–378.

Oxford Diffraction, 2009. CRYSALISCCD and CRYSALISRED in Xcalibur PX software, Oxford Diffraction Ltd., Yarnton, Oxfordshire, England.

Parker, F.S., 1983. Applications of Infrared, Raman and Resonance Raman Spectroscopy in Biochemistry. Plenum Press, New York.

Parr, R.G., Yang, W., 1989. Density-Functional Theory of Atoms and Molecules. Oxford University Press, New York.

Palafox, M.A., Rastogi, V.K., 2002. Quantum chemical predictions of the vibrational spectra of polyatomic molecules. The uracil molecule and two derivatives. Spectrochim. Acta A 58, 411–440.

Podstawka, E., Ozaki, Y., Proniewicz, L.M., 2004. Part I: surface-enhanced Raman spectroscopy investigation of amino acids and their homodipeptides adsorbed on colloidal silver. Appl. Spectrosc. 58, 570–580.

Romani, D., Marquez, M.J., Marquez, M.B., Brandan, S.A., 2015. Structural, topological and vibrational properties of an isothiazole derivatives series with antiviral activities. J. Mol. Struct. 1100, 279–289.

Rostkowska, H., Lapinski, L., Nowak, M.J., 2009. Analysis of the normal modes of molecules with D_{3h} symmetry: infrared spectra of monomeric s-triazine and cyanuric acid. Vib. Spectrosc. 49, 43–51 (Nowak, M.J., Lapinski, L., BALGA computer program for PED calculations).

Sheldrick, G.M., 2008. A short history of SHELX. Acta Crystallogr. A 64, 112–122.

Shukla, N., Lal, A., Singh, V.B., Singh, D.K., 2014. Comparison of DFT methods for molecular structure and vibrational spectrum of pyrimidine molecule. J. Chem. Pharm. Res. 6, 59–69.

Shkurko, O.P., Mamaev, V.P., 1987. The nature of the inductive effect of azinyl groups. Chem. Heterocyc. Compd. 23, 558–562.

Socrates, G., 2001. Infrared and Raman Characteristic Group Frequencies, third ed. John Wiley and Sons Ltd, Chichester, and references therein.

Tayyari, S.F., Rahmatian, R., Tayyari, F., Sammelson, R.E., 2015. Vibrational assignments and proton tunneling studies of pyrimidine–pyrimidinium complex. Sci. Lett. J. 4 (96), 1–11, and references therein.

Umemoto, M., Ogata, T., Shimada, H., Shimada, R., 1984. Polarized Raman and phosphorescence spectra of [$^1H_4$]- and [$^2H_4$]pyrimidines. Bull. Chem. Soc. Jpn. 57, 3300–3306.

Varsányi, G., Szőke, S., 1969. Vibrational Spectra of Benzene Derivatives. Akademiai Kiado, Budapest.

Wang, L., Wen, X., Li, P., Wang, J., Yang, P., Zhang, H., Deng, Z., 2014. 2: 1 5-Fluorocytosine–acesulfame CAB cocrystal and 1: 1 5-fluorocytosine–acesulfame salt hydrate with enhanced stability against hydration. CrystEngCommun 16, 8537–8545.

Yoshii, Y., Sakai, K., Hoshino, N., Takeda, T., Noro, S., Nakamura, T., Akutagawa, T., 2015. Crystal-to-crystal structural transformation of hydrogen-bonding molecular crystals of (imidazolium)(3-hydroxy-2-quinoxalinecarboxylate) through H_2O adsorption–desorption. CrystEngCommun 17, 5962–5969.

Young, N.M., MacKenzie, C.R., Narang, S.A., Oomen, R.P., Baenziger, J.E., 1995. Thermal stabilization of a single-chain Fv antibody fragment by introduction of a disulphide bond. FEBS Lett. 377, 135–139.

Zhurko, G.A., Zhurko, D.A., Chemcraft graphical program for visualization of computed results, <http://www.chemcraftprog.com>.